Proceedings of the ASME 2010 3rd Joint US-European Fluids Engineering Summer Meeting and 8th International Conference on Nanochannels, Microchannels, and Minichannels
FEDSM-ICNMM2010
August 1-5, 2010, Montreal, Canada

FEDSM-ICNMM2010-30537

A COMBINED EXPERIMENTAL AND NUMERICAL STUDY OF FLOW PAST A SINGLE STEP CYLINDER

Chris R. Morton
Mechanical and Mechatronics Engineering
University of Waterloo
Waterloo, Ontario, Canada

Serhiy Yarusevych
Mechanical and Mechatronics Engineering
University of Waterloo
Waterloo, Ontario, Canada

ABSTRACT

The current study investigates flow past a step cylinder for $Re_D = 1050$ and D/d = 2 using both experimental and numerical methods. The focus of the study is on the vortex shedding and vortex interactions occurring in the step cylinder wake. Flow visualization with hydrogen bubble technique and planar Laser Induced Fluorescence has shown that three distinct spanwise vortex cells form: a single vortex shedding cell in the wake of the small cylinder and two vortex shedding cells in the wake of the large cylinder. Vortex connections form between the spanwise vortices in these cells downstream of the step, and vortex dislocations occur at cell boundaries. Complementary to the experimental tests, an LES-RANS hybrid numerical simulation is used to model the flow development. A comparison of the experimental and numerical results indicates that the numerical approach adequately models vortex dynamics in the wake of a step cylinder and, thus, may be used to analyze time dependent, three-dimensional flow topology which is difficult to characterize quantitatively using experimental methods.

INTRODUCTION

Fluid flow around cylindrical bodies has been the focus of a significant number of investigations over the past several decades, e.g., Refs. [1-3]. In most relevant engineering applications, for example, mechanical devices and civil engineering structures, understanding flow development over cylindrical components is of critical importance for engineering design.

Williamson [2] gives a comprehensive review of the flow development over a uniform circular cylinder. The wake of a circular cylinder becomes unstable at about $Re_D = 50$, resulting in a vortex shedding phenomenon. With appropriate boundary conditions, vortices are shed parallel to the cylinder axis in a single cell of constant frequency. Vortex shedding remains two-dimensional for about $50 < Re_D < 190$. As the Reynolds number increases, changes in the vortex shedding pattern occur. In particular, the development of large-scale vortex loops and streamwise vortices takes place for about $190 < Re_D < 240$, and smaller-scale streamwise vortices form for $Re_D \approx 240$ and beyond. The streamwise vortices form in pairs, and are persistent for Reynolds numbers up to and within the shear layer transition regime [2].

Investigations of the flow development past complex cylindrical geometries are far less common than those pertaining to uniform circular cylinders. Such complex geometries (e.g., cantilevered, tapered, and step cylinders) produce similar flow features to those observed for a uniform circular cylinder. In particular, it has been shown that in uniform flows spanwise vortices are shed in constant-frequency cells in the wakes of cantilevered [4,5], tapered [6,7], and step cylinders [8-12]. The arrangement of the vortex cells and wake vortex interactions, however, depend significantly on the geometry. For example, multiple vortex shedding cells develop across the span of tapered cylinders [6]. For cantilevered cylinders, a lower frequency vortex shedding cell forms near the free end, and a higher frequency cell, similar to vortex shedding in the wake of a uniform circular cylinder, is observed away from the free end [4]. Finally, for a step cylinder (Fig. 1), vortex shedding cells develop in the wakes of the smaller cylinder and the larger cylinder and may interact in the wake downstream of the step [11,12]. Complex vortex interactions, i.e., vortex dislocations [13] or vortex splitting [14], take place at the cell boundaries; however, there seem to be some discrepancies between such interactions observed on different geometries (e.g., Refs. [11-16]).

The present investigation is focused on the flow development over a step cylinder (Fig. 1), as this relatively simple geometry allows studying complex vortex interactions. The flow development in the wake of a step cylinder is

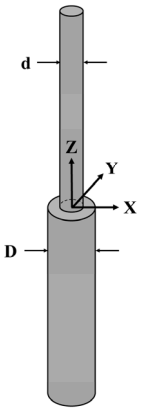

FIG 1. DIAGRAM OF THE STEP CYLINDER.

dependent on the Reynolds number (Re_D) and the ratio of the large cylinder diameter (D) to the small cylinder diameter (d), referred to as the diameter ratio (D/d). Previous experimental studies suggest that, due to a mismatch between the shedding frequencies of the small and the large cylinders, vortex interactions take place in a wake region downstream of the step. Ko, Leung, and Au [8] identified such an interaction region of non-uniform shedding downstream of the step, which was offset towards the large cylinder. Vortex interactions within this region were the topic of several subsequent investigations [9-12]. Lewis and Gharib [11] identified two different modes of vortex shedding downstream of the step, namely, the 'direct mode' and the 'indirect mode'. In the direct mode (D/d < 1.25), the vortex interaction region is relatively narrow, with vortex connections occurring between vortices shed from the large and the small cylinders and vortex dislocations involving connections between vortices in the same cell. The D/d boundary defining this mode was found to be dependent on Re_D. In the indirect mode (D/d > 1.55), a distinct vortex shedding frequency, different from the dominant vortex shedding frequencies in the wakes of the large and the small cylinders, was detected within the interaction region [11]. This frequency was found to be the lowest of the three shedding frequencies and was attributed to a distinct vortex shedding phenomenon occurring in the interaction region. Adopting terminology introduced by Dunn and Tavoularis [12], three types of wake vortex shedding patterns can be identified in the wake of a step cylinder: (i) the S-cell – vortex shedding from the small cylinder; (ii) the L-cell – vortex shedding from the large cylinder; (iii) the N-cell – distinct vortex shedding in the region between the S-cell and the L-cell. Based on flow visualization results, Lewis and Gharib [11] and Dunn and Tavoularis [12] suggest that the N-cell is a cyclic phenomenon. That is, the formation of N-cell vortices interrupts periodically and then resumes after a few L-cell shedding cycles. However, the mechanism behind the N-cell formation and its cyclical nature remains unexplained.

Recent experimental studies focused on vortex dynamics in the wake of a step cylinder have been limited to the laminar vortex shedding regime [11,12]. In addition, to the best knowledge of the authors, the only two published numerical studies for this geometry [17,18] were also performed for the laminar shedding regime. The present study is motivated by the need for improved understanding of vortex dynamics in the wake of a step cylinder in the turbulent shedding regime, which is more common in relevant engineering applications. The main objective is to investigate experimentally and numerically the vortex shedding in the wake of a step cylinder for D/d = 2 and $Re_D = 1050$.

NOMENCLATURE

A	=	frontal area of the cylinder
C_D	=	drag coefficient, $F_D/0.5\rho AU^2$
D	=	large cylinder diameter
d	=	small cylinder diameter
F_D	=	drag force in X direction
f	=	vortex shedding frequency
f_{EL}	=	vortex shedding frequency of the EL-cell
f_{ES}	=	vortex shedding frequency of the ES-cell
f_L	=	vortex shedding frequency of the L-cell
f_N	=	vortex shedding frequency of the N-cell
f_S	=	vortex shedding frequency of the S-cell
L	=	span of the cylinder
Re_D	=	Reynolds number, UD/ν
Q	=	second invariant of the velocity gradient tensor
St	=	Strouhal number, fD/U
t	=	time
t*	=	dimensionless time, tf_L
U	=	free-stream velocity
u, v, w	=	streamwise, transverse, and spanwise velocity components
X,Y,Z	=	streamwise, transverse, and spanwise coordinates
Δt	=	time step size in (s) for simulations
ρ	=	density
ν	=	kinematic viscosity

EXPERIMENTAL METHOD

All experiments were carried out in a water flume facility in the Fluid Mechanics Research Laboratory at the University of Waterloo. The 2.0 m long test section of the flume has a height of 1.2 m and a width of 1.2 m. During the experiments, the water level was maintained at 0.8 m, and the background turbulence intensity was less than 1%. The step cylinder was mounted between two endplates, designed following recommendations of West and Fox [19]. The flume was operated at a free stream speed of 87mm/s, with a flow uniformity within 2.3%. Figure 2 shows the experimental arrangement of the step cylinder and the end plates, as well as relevant dimensions of the cylinder. To visualize wake vortices, a hydrogen bubble technique and planar Laser Induced Fluorescence (LIF) were employed. The flow was illuminated using a laser sheet generated by a 2W continuous wave laser. Hydrogen bubbles were produced on a thin (0.09 mm diameter) stainless steel wire mounted approximately 0.2D upstream of

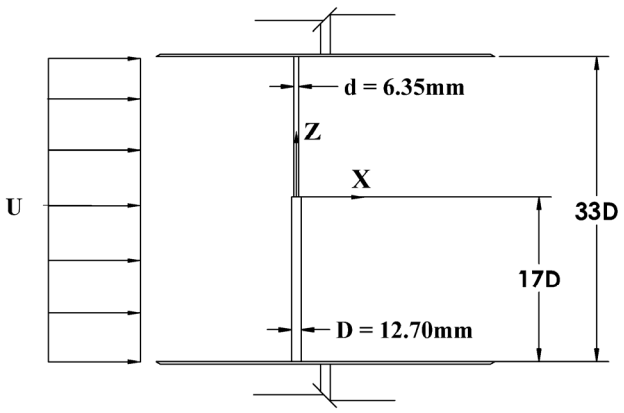

FIG 2. EXPERIMENTAL ARRANGEMENT.

the step cylinder along its entire span, similar to the arrangement used by Kappler et al. [20] for a uniform cylinder. With a DC voltage applied to the stainless steel wire, a continuous sheet of bubbles is generated in the X-Z plane. The size of bubbles and hence, their buoyancy depend on the wire diameter and the applied voltage [21]. For the parameters employed in this study, it was verified experimentally that buoyancy effects were negligible, i.e., could not be detected with flow visualization.

For planar LIF visualization, Rhodamine dye was injected from a small probe placed about 20D upstream of the cylinder axis. The dye was illuminated in the X-Y plane to visualize wake vortex shedding, and in the X-Z plane to visualize flow near the step. When visualizing vortex shedding in the X-Y plane, the dye injection and hydrogen bubble systems were used simultaneously (Fig. 3). This allowed correlating the planar LIF images obtained in the X-Y plane to the spanwise development of wake vortices monitored in the X-Z plane. In addition, vortex cores were easier to identify in the planar images. For hydrogen bubble visualizations, spanwise vortices on one side of the wake were illuminated in the X-Z plane with a laser sheet positioned at $Y/D \approx -0.375$.

Flow visualization images were obtained with a Nikon D300 camera. In addition, another camera was used to record videos simultaneously with sequences of still images to aid in the identification of periodic phenomena in the wake.

COMPUTATIONAL METHOD

Numerical modeling was based on Detached Eddy Simulation (DES), which combines Large Eddy Simulation (LES) and Unsteady Reynolds Averaged Navier Stokes (URANS) methods. A comprehensive review of this method is given by Spalart [22]. Although DES is a relatively new technique, it has been applied to model the flow development over uniform circular cylinders and the results have shown an improved agreement with experiments compared to traditional RANS-based models, e.g., Refs. [23, 24]. In this study, the

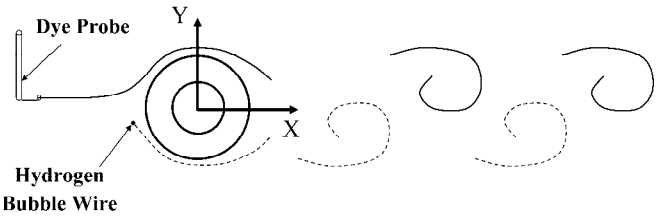

FIG 3. FLOW VISUALIZATION SETUP.

SST-DES model developed by Menter [25] was employed using the ANSYS CFX 12.0 solver.

The computational domain is shown in Fig 4, with the origin of the coordinate system located on the cylinder axis at the step. The inlet boundary is placed 10D upstream and the outlet boundary is placed 20D downstream from the centre of the cylinder. The transverse boundaries are placed 8D from the cylinder centre. The spanwise depth of the domain is 19D, with the large and small cylinders occupying 15D and 4D, respectively. The domain size is comparable to that used by Narasimhamurthy et al. [7] for modeling flow over a tapered cylinder.

At the inlet boundary, a uniform velocity profile and Neumann boundary condition for pressure is employed; whereas, at the outlet, a Neumann boundary condition for the

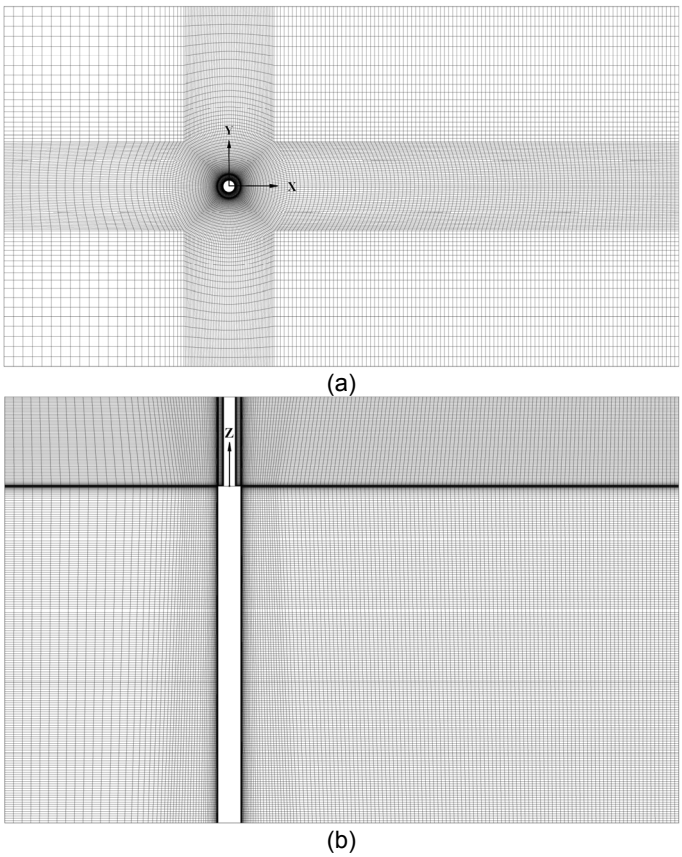

FIG 4. COMPUTATIONAL DOMAIN.

velocity and a constant (zero) pressure are applied. At other domain boundaries, a free-slip condition is applied, and a no-slip condition is applied at the model surface.

A structured O-grid mesh was employed, with mesh refinement carried out in two phases. First, the mesh for the regions away from the step was selected based on a mesh independence study completed for a three-dimensional uniform cylinder with an in-plane depth of 3D and the same planar (X-Y) dimensions as those in Fig. 4a. Mesh configurations were investigated primarily for Re_D = 1050, corresponding to flow past the large cylinder, since the results would be applicable to the small cylinder operating at Re_D = 525. To ensure convergence of the numerical results, each configuration was run for more than 30 vortex shedding cycles. Based on the drag coefficient and Strouhal number results presented in Table 1, mesh configuration 2 was selected for both the large and the small cylinder. The corresponding two-dimensional mesh density and spanwise mesh spacing is comparable to that used by Nishino [23] for modeling flow development past a uniform circular cylinder in ground effect.

In the second phase of mesh refinement, the spanwise mesh density in a region surrounding the step is increased to resolve boundary layer and shear layer development. Specifically, the spanwise mesh spacing at the step and its gradual relaxation away from the step matches the corresponding radial mesh spacing at the cylinder surfaces and the relaxation in the radial direction away from the cylinder. As a result, on the large cylinder side, 34 spanwise cells were located within $-0.75 \le Z/D \le 0$. On the small cylinder side, 29 spanwise cells were located within $0 \le Z/D \le 0.375$. The final mesh contained approximately 5.6×10^6 elements.

All numerical data presented were acquired after steady spanwise vortex shedding in the wakes of the large and small cylinders was attained in the simulations.

RESULTS

The results have been divided into three sections. First, experimental and numerical results for flow past uniform circular cylinders at Re_D = 525 and Re_D = 1050 are presented. In the second section, experimental data pertaining to flow past a step cylinder at Re_D = 1050 and D/d = 2 are discussed. The overall flow development is investigated, and the results are compared to those from previous experimental studies. Finally, the numerical results pertaining to the flow past a step cylinder at Re_D = 1050 and D/d = 2 are compared with the experimental findings to validate the numerical method employed.

Flow Development over Uniform Circular Cylinders

The two uniform cylinders investigated corresponded to the large (diameter, D) and the small (diameter, d) cylinders in the step cylinder configuration (D/d = 2). The cylinders were tested for Re_D = 1050 and Re_D = 525. Uniform cylinders were located between the endplates (Fig. 2), with aspect ratios of 33 and 66 for the large and small cylinder, respectively.

TABLE 1 MESH INVESTIGATION RESULTS FOR A UNIFORM CIRCULAR CYLINDER.

Mesh Config.	X-Y Cells[1]	ΔZ Cells[2]	Time Step, ΔtU/D	Re_D	C_D	St
1	25000	20	0.006	1050	1.199	0.22
1	25000	20	0.012	1050	1.199	0.223
2	25000	30	0.012	1050	1.179	0.221
3	25000	60	0.012	1050	1.174	0.22
4	50000	60	0.012	1050	1.160	0.22
2	25000	30	0.012	525	1.227	0.228
Experiment [3,26]	-	-	-	1050	0.97	0.210
	-	-	-	525	1.02	0.205

[1]The total number of cells in each X-Y planar mesh
[2]The total number of spanwise cells in the computational domain

Figures 5a-d show hydrogen bubble and LIF flow visualization images. Away from the endplates, nearly parallel vortex shedding is observed (Figs. 5a and 5c). Planar LIF images (Figs. 5b and 5d) reveal a common vortex street in the core of the flow. Similar to previous experimental studies, e.g., Refs. [27, 28], vortex shedding was affected near endplates, with end cells forming within about 4-5 diameters from each endplate. An analysis of video records revealed that, apart from

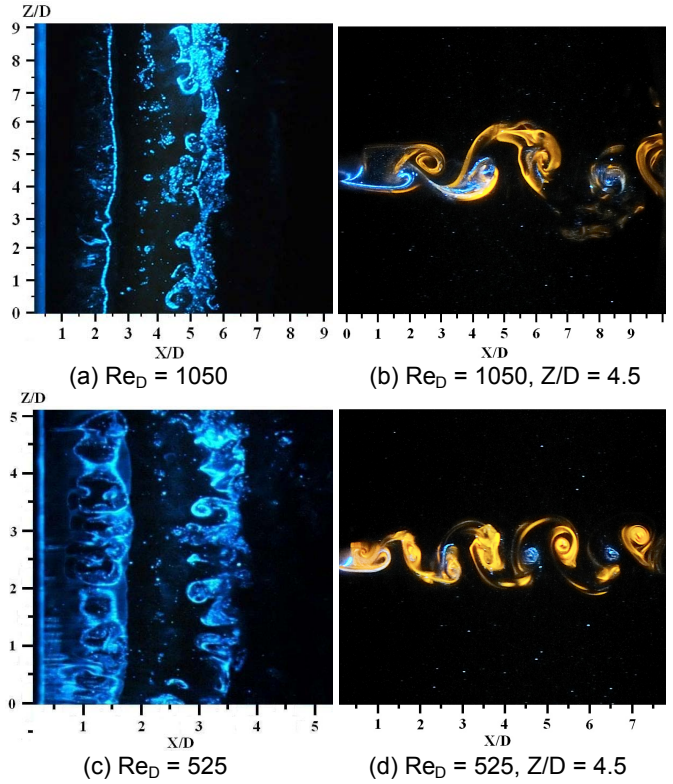

FIG 5. EXPERIMENTAL RESULTS OF VORTEX SHEDDING IN THE WAKE OF A UNIFORM CIRCULAR CYLINDER AT Re_D = 1050 AND Re_D = 525.

the end cells, the shedding frequency is constant along the span of the cylinders, with St = 0.203 and St = 0.198 for the large and small cylinder, respectively. These values are in agreement with previous experimental results reported by Norberg [3]. In comparison, the SST-DES results (Table 1) give St = 0.221 and St = 0.228 for the large and small cylinder, respectively. These values are within about 10% of the experimental results reported by Norberg [3], and agree with previous SST-DES simulations (e.g., Refs. [24,29]).

Flow visualization images in Figs. 5a and 5c reveal three-dimensional structures known to occur in the wake of a uniform cylinder at the investigated Reynolds numbers [30]. Using flow visualization techniques similar to those shown in Figs. 5a and 5c, Wu et al. [30] described three-dimensional "mushroom-type structures" which appear along the cylinder axis in the near wake region. Evidence of these structures can be seen, for example, in Fig. 5a at X/D = 5.0 and Z/D = 7.25, and in Fig. 5c at X/D = 3.25 and Z/D = 3.5.

Numerical simulation results for a uniform cylinder at Re_D = 1050 are presented in Figs. 6a-c, all of which pertain to the same instant in the simulation. Numerical flow visualization with isosurfaces of $Q \approx 0.1U^2/D^2$ [31] is shown in Fig. 6a. The resolved structures in the wake are in agreement with previous DES studies on uniform circular cylinders [23,24]. Specifically, similar to experimental results [30], numerical results reveal the formation of streamwise vortices in the near wake. For comparison, contours of total vorticity magnitude are shown in Figs. 6b and 6c at X-Z and X-Y planes matching the position of the laser sheets in the flow visualization images presented in Figs. 5a and 5b. The numerical results are in good agreement with the corresponding flow visualization results in Fig. 5a and 5b. Comparing Figs. 6a and 6b, it can be seen that the three-dimensional streamwise vortices leave a distinct footprint on a planar vorticity plot, for example, at X/D = 2.5 and Z/D = 1.25, 1.75, 2.25 and 2.75.

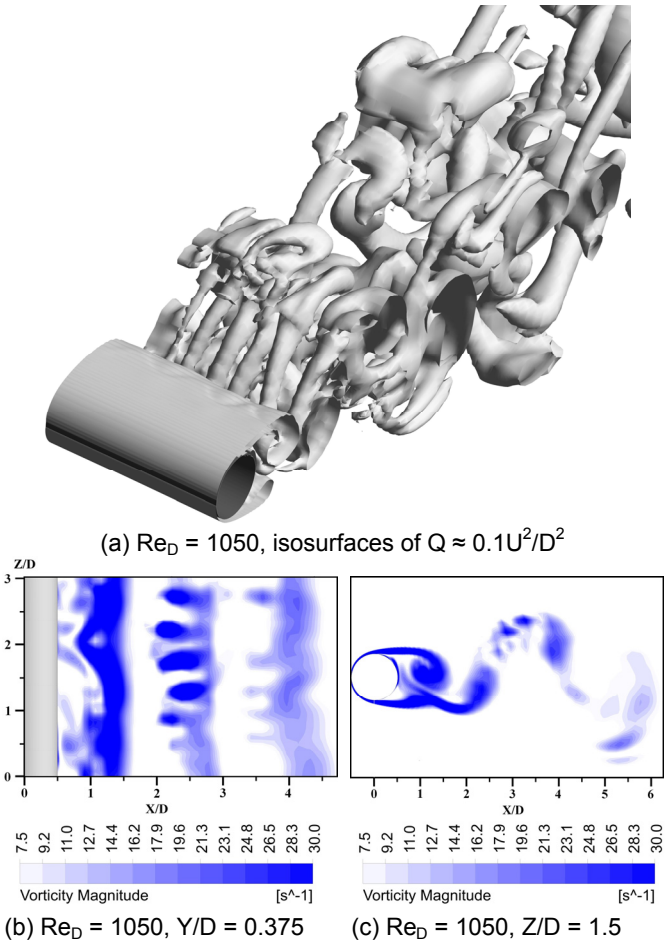

FIG 6. DES RESULTS OF VORTEX SHEDDING IN THE WAKE OF A UNIFORM CIRCULAR CYLINDER AT Re_D = 1050.

Flow Development over a Step Cylinder

The flow development over a step cylinder is illustrated in Figs. 7a-e with a sequence of hydrogen bubble flow visualization images. In agreement with experimental results by Lewis and Gharib [11] and Dunn and Tavoularis [12], three distinct spanwise vortex shedding cells can be identified in the wake of the step cylinder: (i) the S-cell, vortex shedding from the small cylinder, (ii) the L-cell, vortex shedding from the large cylinder, and (iii) the N-cell, which appears cyclically near the step on the large cylinder side, e.g., $-7 \le Z/D \le 0$. As expected, the vortex shedding frequency in the S-cell is higher than that in the L-cell or N-cell, which is evidenced by a higher number of vortices in the wake of the small cylinder.

To investigate the N-cell development, it is instructive to focus on the wake of the large cylinder. Figure 7a shows nearly parallel vortex shedding in the wake of the large cylinder. Over time, vortices in the large cylinder wake become inclined towards the step (Fig. 7b). Eventually, a distinct vortex shedding cell (N-cell) can be observed near the step (Fig. 7c), which is bordered by the large and small cylinder vortices below and above, respectively. The N-cell vortices continue to move out of phase with the L-cell vortices until a vortex dislocation occurs, for example, the L-cell vortex at $X/D \approx 5$ in Fig. 7d maintains a weak connection with its counterpart in the N-cell, while the N-cell vortex connects primarily to the upstream L-cell vortex at $X/D \approx 2.5$. The N-cell vortices re-align in phase with the large cylinder vortices (Fig. 7e), and the N-cell becomes difficult to distinguish from the L-cell via flow visualization. In Fig. 7e, vortex shedding in the large cylinder wake occurs at an angle away from the step; however, after a few shedding cycles, the spanwise vortices are again shed parallel with the cylinder axis, marking the beginning of the next N-cell cycle. Despite the presence of three-dimensional structures in the step cylinder wake, the results suggest that the N-cell development agrees qualitatively with that observed in the laminar shedding regime by Dunn and Tavoularis for Re_D = 152, and $D/d \approx 2$ [12].

Due to the difference in shedding frequencies between adjacent vortex cells, vortex dislocations occur at the cell boundaries, resulting in intricate vortex connections. It should

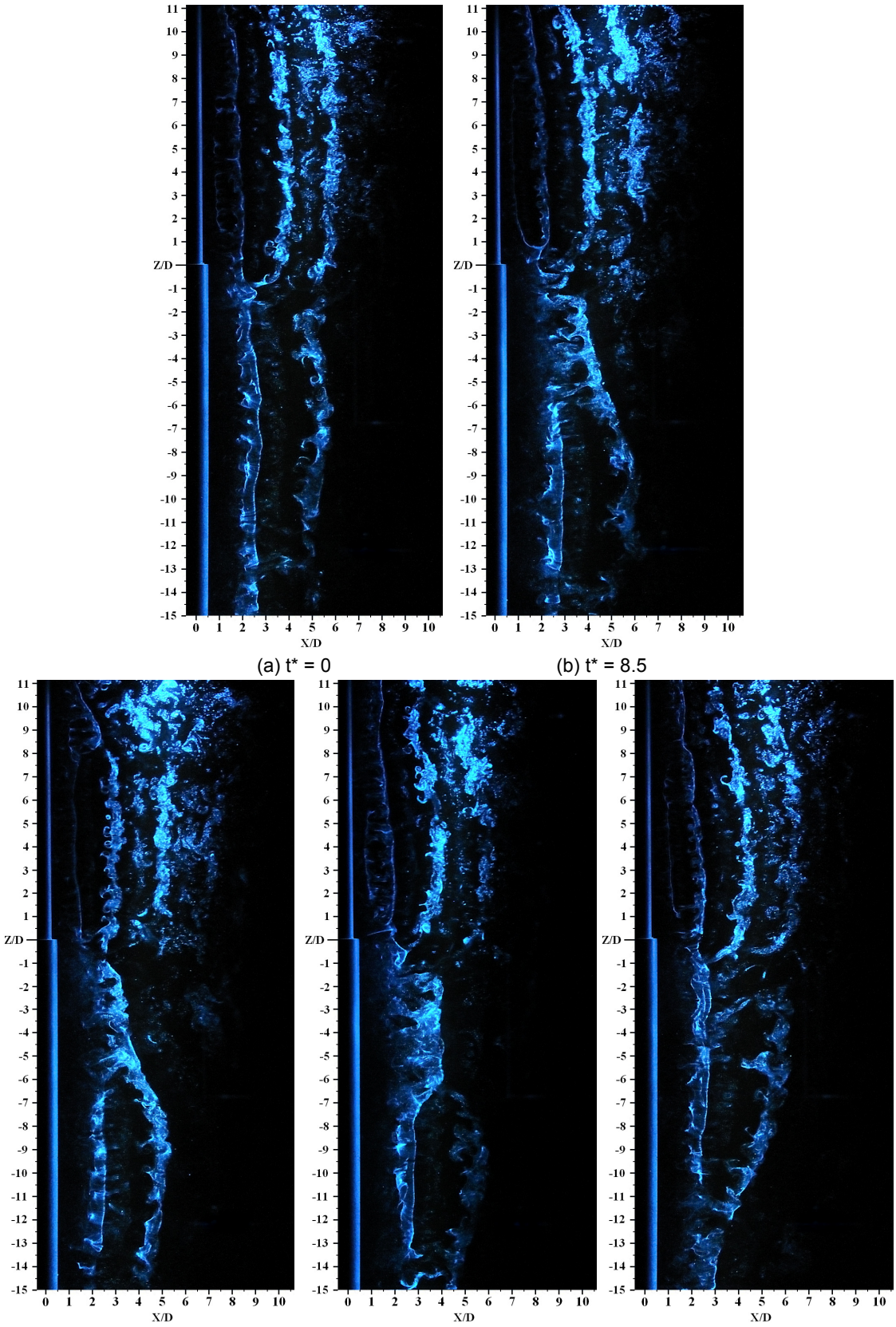

(a) t* = 0 (b) t* = 8.5

(c) t* = 18.2 (d) t* = 21.3 (e) t* = 23.4

FIG 7. VORTEX SHEDDING IN THE STEP CYLINDER WAKE.

be noted that vortex dislocations cause the locations of the cell boundaries to fluctuate with time. Near each endplate, a low frequency vortex shedding cell was observed, similar to the end cells observed for uniform cylinders. These cells are referred to as: (i) the ES-cell, vortex shedding near the small cylinder boundary, and (ii) the EL-cell, vortex shedding near the large cylinder boundary.

Estimations of the shedding frequency for each vortex shedding cell are shown in Fig. 8, where the maximum observed spanwise extent of each cell is identified. The shedding frequencies were estimated based on an analysis of video records capturing over 500 L-cell shedding cycles. Based on the results presented in Fig. 8, the following transition regions between distinct cells along the span of the cylinder can be identified at a given downstream location: (i) the S-ES cell boundary, (ii) the N-S cell boundary, (iii) the N-L cell boundary, and (iv) the L-EL cell boundary. Within these transition regions, vortex splitting occurs, resulting in intricate vortex connections. At the N-S cell boundary, S-cell vortices often form direct vortex connections with N-cell vortices (Fig. 7a). The analysis of video records revealed that the remaining S-cell vortices form half-loop connections with vortices shed on the opposite side of the wake, agreeing with Dunn and Tavoularis [11]. Due to this, the S-cell vortices are oriented in the streamwise direction near the step (Fig. 7e). At the N-L cell boundary, N-cell vortices frequently form direct connections with L-cell vortices (Fig. 7b). However, when N-cell vortices

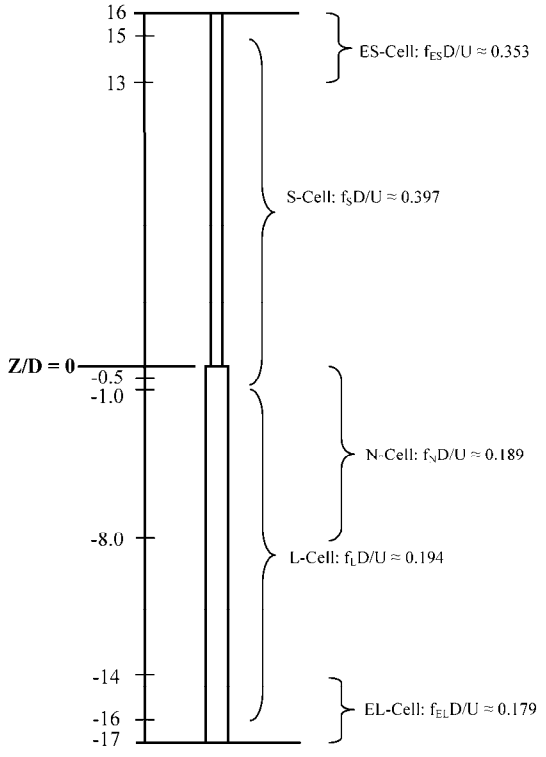

FIG 8. DIMENSIONLESS VORTEX SHEDDING FREQUENCY ACROSS THE SPAN.

are out of phase with L-cell vortices, they split into at least two vortex filaments, forming vortex connections with two consecutive L-cell vortices on the same side of the wake (Fig. 7c and 7d).

It is of interest to investigate the effect of the Reynolds number on flow characteristics. Using LDV measurements and/or flow visualization, Dunn's [32] results showed that the average spanwise extent of the N-cell decreases with increasing the Reynolds number for $152 \leq Re_D \leq 621$ and D/d = 1.98. Norberg [10], reports the same trend for $Re_D = 3x10^3 – 13x10^3$ and D/d = 2. Table 2 facilitates a quantitative analysis between the results from Dunn [32], Dunn and Tavoularis [12], and the current study. It should be noted that the extent of the N-cell shown in Fig. 8 (approximately 8D) is the maximum observed spanwise extent. The average span of this cell is considerably smaller and was estimated to be 3-5D based on video records (Table 2). The results in Table 2 also show that the increase in the Reynolds number is accompanied by an increase in f_N/f_L. However, the observed increase in f_N/f_L is checked.

Changes in the vortex shedding pattern along the span of the step cylinder are depicted in Fig. 9. The flow visualization images presented illustrate typical flow patterns seen within the S-cell (Fig. 9b), the N-S cell boundary (Fig. 9c), the N-cell (Fig. 9d), the N-L cell boundary (Fig. 9e), and the L-cell (Fig. 9f). Periodic vortex shedding, similar to that observed for uniform cylinders, is seen within the S-cell, N-cell, and L-cell (Figs. 9b, 9d, and 9f). In contrast, at the cell boundaries, vortex interactions result in a dramatically different pattern (Figs. 9c and 9e).

Variations in vortex shedding pattern at the N-S cell boundary are illustrated in Figs. 10a and 10b, showing two images captured at the same spanwise location, Z/D = -0.5, but at different instances in the shedding cycle. In Fig. 10a and 10b, S-cell vortices can be seen for $X/D \geq 2$ and $X/D \geq 4$, respectively. On the other hand, N-cell vortices appear in Fig. 10a for $X/D < 2$, while more complex flow structures characteristic of the N-S cell boundary can be seen in Fig. 10b for $X/D < 4$. The observed changes in the vortex shedding pattern occur frequently, suggesting that the location of the N-S cell boundary fluctuates rapidly. Such fluctuations are attributed to vortex dislocations, which are expected to occur at a frequency of (f_S-f_N) at the N-S cell boundary [18]. In addition, low frequency downwash fluctuations, that have been shown to be linked to the N-cell development, may also play a role [18].

TABLE 2 N-CELL EXERIMENTAL DATA

Experimental Study	Re_D	D/d	Average N-cell extent	f_N/f_L
Dunn and Tavoularis [11]	152	1.98	13.0D	0.84
Dunn [31]	296	1.98	6.8D	0.94
Dunn [31]	621	1.98	5.6D	0.96
Current Study	1050	2	3-5D	0.97

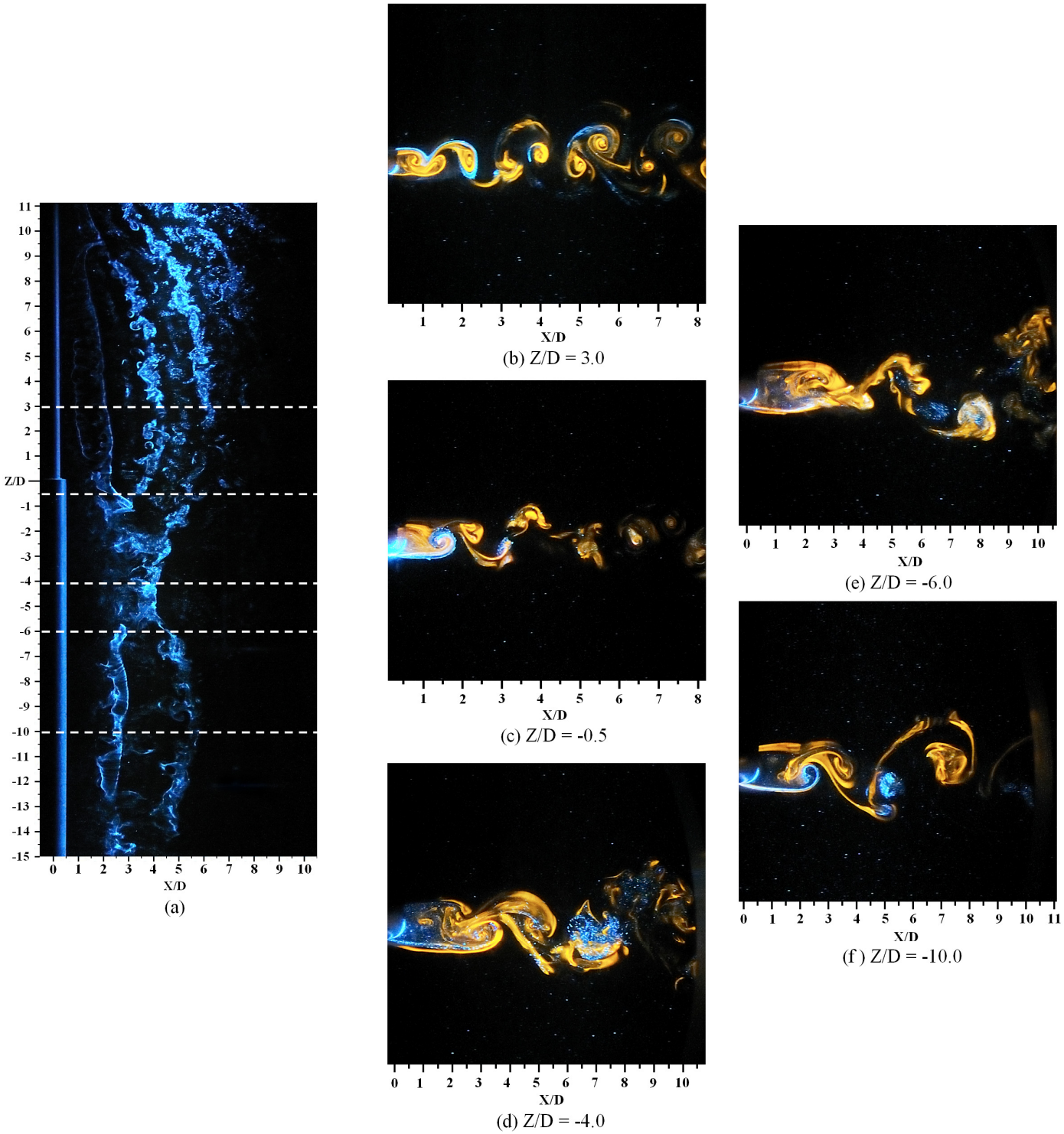

FIG 9. VORTEX SHEDDING PATTERNS AT DIFFERENT LOCATIONS ALONG THE SPAN.

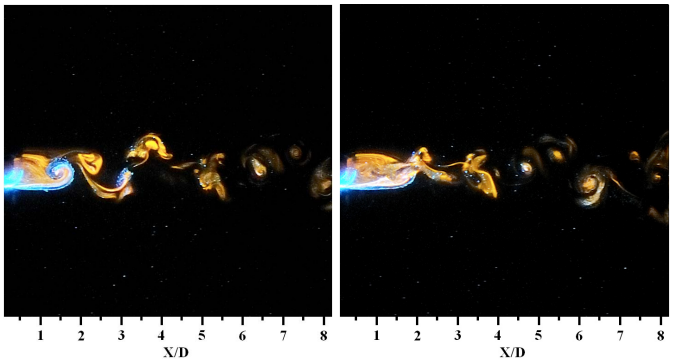

(a) t* = 0 (b) t* = 2.3

FIG 10. CHANGES IN THE VORTEX SHEDDING PATTERN AT THE N-S CELL BOUNDARY.

A sequence of images in Fig. 11 illustrates the presence of a downwash over the step and a strong three-dimensionality of the flow in this region. Here, dye was illuminated with a laser sheet oriented in the X-Z plane near the wake centre line. The images show dye being entrained into the large cylinder wake, visualizing rather intricate small-scale, three-dimensional structures. Such structures are likely forming due to the interaction of streamwise and spanwise vortices downstream of the step.

Numerical Results of Flow over a Step Cylinder

Numerical simulation results have been computed for several L-cell vortex shedding cycles after steady state vortex shedding was established. To facilitate a comparison between the numerical and experimental results, Fig. 12a shows contours of total vorticity magnitude in the X-Z plane whose Y/D location matches the position of the laser sheet used in the hydrogen bubble flow visualization experiments (Fig. 12b). The instantaneous image in Fig. 12a was selected to approximately match the shedding cycle phase of the results in Fig. 12b. In agreement with the flow visualization image, three distinct vortex shedding cells can be identified in Fig. 12a: the N-cell ($-4.5 \leq Z/D \leq 0$), the L-cell ($Z/D \leq -5$), and the S-cell ($Z/D \geq 0$). Three L-cell vortices can be identified for $Z/D \leq -5$ in the large cylinder wake, with vortices at $X/D \approx 1.5$ and $X/D \approx 4.5$ being of the same sign (Fig. 12a). It can be seen that the N-cell vortex, located within $-4.5 \leq Z/D \leq 0$ and $X/D \approx 2$, is split into at least two vortex filaments, and forms direct vortex connections with two L-cell vortices of the same sign. The vortex connections and locations of the cell boundaries are in good agreement with the flow visualization results presented in Fig. 12b.

A three-dimensional visualization of the flow is shown in Fig. 12c Similar to the experimental results presented in Fig. 7, the numerical results reveal the formation of streamwise vortices. In contrast to previous investigations on this geometry performed in the laminar regime [17,18], the presence of such structures dramatically changes the flow topology, significantly

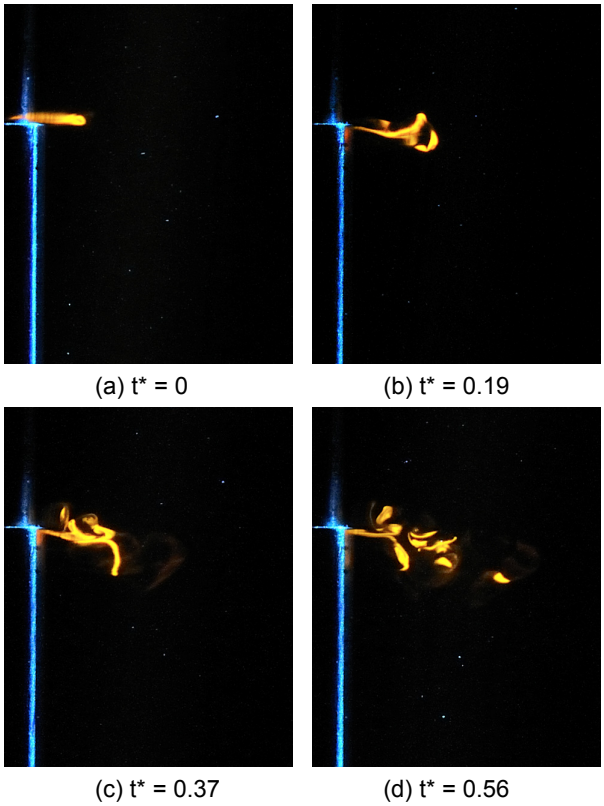

(a) t* = 0 (b) t* = 0.19

(c) t* = 0.37 (d) t* = 0.56

FIG 11. PRESENCE OF DOWNWASH AT THE STEP.

complicating vortex interactions taking place between the neighboring spanwise vortex cells.

Changes in the vortex shedding pattern along the span of the step cylinder are depicted in Fig. 13, which show contours of total vorticity in several X-Y planes. The images were captured at the same time as the results presented in Figs. 12a and 12c, approximately corresponding to the same phase in the N-cell cycle as that in Fig. 9a. Comparing the images in Fig. 13 with the corresponding images in Fig. 9, there is good agreement between numerical and experimental results within each cell and at the cell boundaries. The presented numerical results suggest that DES can be employed to gain added insight into the 3D flow topology, which is difficult to characterize using experimental methods.

CONCLUSIONS

Vortex shedding in the wake of a step cylinder was investigated experimentally and numerically for $Re_D = 1050$ and $D/d = 2$. Although the study was completed in the turbulent shedding regime, many similarities were found with experimental investigations completed at Reynolds numbers pertaining to the laminar shedding regime (e.g., Refs. [11,12]). In particular, experimental and numerical results show that three distinct spanwise vortex shedding cells form in the step cylinder wake: the S-cell, N-cell, and L-cell. The N-cell, which forms in a region downstream of the step on the large cylinder side, has the lowest shedding frequency of the three cells. Due

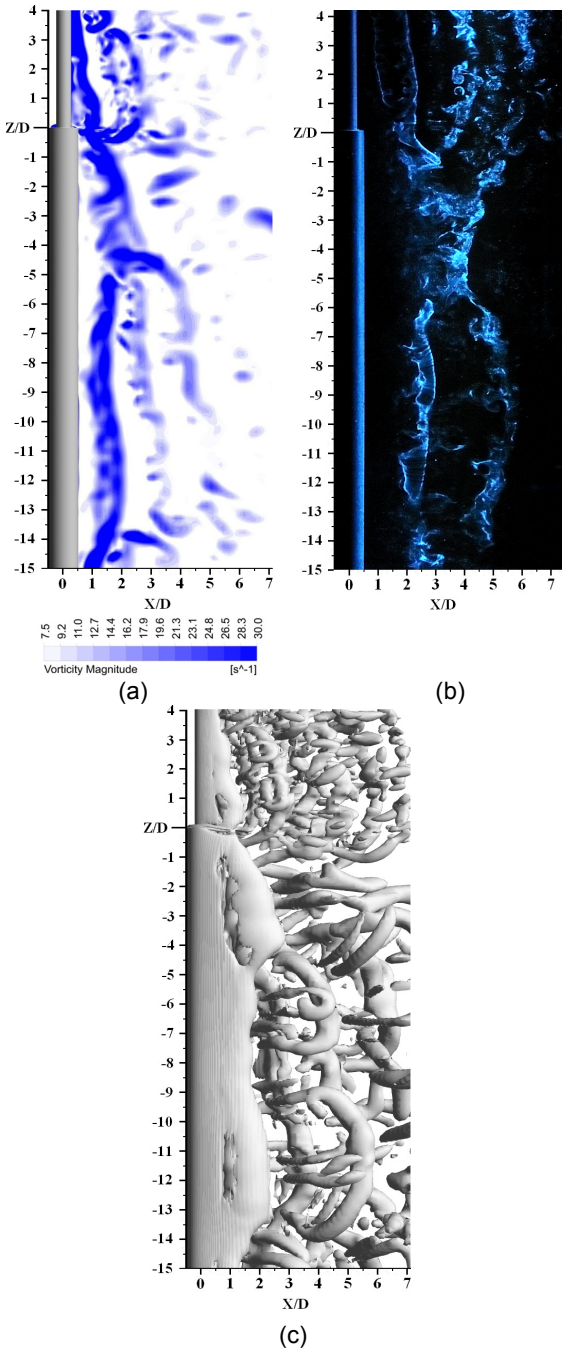

FIG 12. VORTEX SHEDDING IN THE WAKE OF A STEP CYLINDER AT Re_D = 1050 AND D/d = 2: (a) CONTOURS OF TOTAL VORTICITY MAGNITUDE, (b) HYDROGEN BUBBLE FLOW VISUALIZATION, AND (c) ISOSURFACES OF Q ≈ $0.1U^2/D^2$.

to the difference in shedding frequencies of the N-cell, L-cell, and S-cell, vortex connections and dislocations take place at the cell boundaries. At the N-S cell boundary, S-cell and N-cell vortices often form direct vortex connections, while additional S-cell vortices form half-loop connections with a nearby S-cell vortex of the same sign. At the N-L cell boundary, N-cell and L-cell vortices consistently form direct vortex connections. When the N-cell and L-cell vortices are out of phase, N-cell vortices split to facilitate such direct connections. The presence of vortex dislocations at the N-S and N-L cell boundaries causes their spanwise position to fluctuate with time. As a result, the vortex shedding pattern within each of the cell boundaries varies with time.

A quantitative comparison of the results obtained in the present investigation and those from previous experimental studies suggests that, for a given diameter ratio, the average extent of the N-cell decreases with an increase of the Reynolds number. In addition, this is accompanied by an increase in the ratio of the N-cell and L-cell shedding frequencies, f_N/f_L. The increase in f_N/f_L is limited, however.

While the observed cellular vortex shedding in the wake of a step cylinder for Re_D = 1050 is comparable to that found in the laminar shedding regime, the attendant formation of smaller scale streamwise vortices complicates the flow topology and the interactions between the spanwise vortices in neighboring cells. The DES results illustrate the complexity of the turbulent wake forming behind a step cylinder. The presence of three-dimensional structures in the wake can be expected to influence wake vortex shedding characteristics, and such influence should be quantified in future investigations.

ACKNOWLEDGMENTS

The authors gratefully acknowledge the Natural Sciences and Engineering Research Council of Canada (NSERC) for funding of this work.

REFERENCES

[1] Gerrard, G.H., 1978, "The wakes of cylindrical bluff bodies at low Reynolds number," Philosophical Transactions of The Royal Society of London **A 288**, pp. 351-382.

[2] Williamson, C.H.K., 1996, "Vortex dynamics in the cylinder wake," Annual Review of Fluid Mechanics **28**, pp. 477-539.

[3] Norberg, C., 2003, "Fluctuating lift on a circular cylinder: review and new measurements," Journal of Fluids and Structures **17**, pp. 57-96.

[4] Ayoub, A., and Karamcheti, K., 1982, "An experiment on the flow past a finite circular cylinder at high subcritical and supercritical Reynolds numbers," Journal of Fluid Mechanics **118**, pp. 1-26.

[5] Afgan, I., Moulinec, C., Prosser, R., and Laurence, D., 2007, "Large eddy simulation of turbulent flow for wall mounted cantilever cylinders of aspect ratio 6 and 10," International Journal of Heat and Fluid Flow **28**, pp. 561-574.

[6] Gaster, M., 1969, "Vortex shedding from slender cones at low Reynolds numbers," Journal of Fluid Mechanics **38**, pp. 565-576.

[7] Narasimhamurthy, V.D., Andersson, H. I., and Pettersen, B., 2009, "Cellular vortex shedding behind a tapered circular cylinder," Physics of Fluids **21**, pp. 1-12.
[8] Ko, N.W.M., Leung, W.L., and Au, H., 1982, "Flow behind two coaxial circular cylinders," ASME Journal of Fluids Engineering **104**, pp. 223-227.
[9] Yagita, M., Kojima, Y., and Matsuzaki, K., 1984, "On vortex shedding from circular cylinder with step," Bulletin of JSME **27**(225), pp. 426-430.
[10] Norberg, C., 1992, "An experimental study of the flow around cylinders joined with a step in diameter," 11th Australasian Fluid Mechanics Conference, Hobart, Austrailia, pp. 507-510.
[11] Lewis, C.G., and Gharib, M., 1992, "An exploration of the wake three dimensionalities caused by a local discontinuity in cylinder diameter," Physics of Fluids A **4**, pp. 104-117.
[12] Dunn, W., and Tavoularis, S., 2006, "Experimental studies of vortices shed from cylinders with a step-change in diameter," Journal of Fluid Mechanics **555**, pp. 409-437.
[13] Williamson, C.H.K., 1989, "Oblique and parallel modes of vortex shedding in the wake of a cylinder," Journal of Fluid Mechanics **206**, pp. 579-627.
[14] Eisenlohr, H., and Eckelmann, H., 1989, "Vortex splitting and its consequences in the vortex street wake of cylinders at low Reynolds numbers," Physics of Fluids A **1**, pp. 189-192.
[15] Williamson, C. H. K., 1992, "The natural and forced formation of spot-like 'vortex dislocations' in the transition of a wake," Journal of Fluid Mechanics **243**, pp. 393-441.
[16] Piccirillo, P.S., and Van Atta, C.W., 1993, "An experimental study of vortex shedding behind linearly tapered cylinders at low Reynolds number," Journal of Fluid Mechanics **246**, pp. 163-195.
[17] Valles, B., Andersson, H.I., and Jenssen, C.B., 2002, "Direct-mode interactions in the wake behind a stepped cylinder," Physics of Fluids **14**, pp. 1548-1551.
[18] Morton, C., Yarusevych, S., 2010, "Vortex shedding in the Wake of a Step Cylinder," submitted to Physics of Fluids.
[19] West, G.H., and Fox, T.A., 1990, "On the use of end plates with circular cylinders," Experiments in Fluids **9**, pp. 237-239.
[20] Kappler, M., Rodi, W., Szepessy, S., and Badran, O., 2005, "Experiments on the flow past long circular cylinders in a shear flow," Experiments in Fluids, **38**, pp. 269-284.
[21] Lian, Q.X., and Su, T.C., "The Application of Hydrogen Bubble Method in the Investigation of Complex Flows," Atlas of Flow Visualization II, CRC Press, Chap. 6.
[22] Spalart, P. R., 2009, "Detached Eddy Simulation," Annual Review of Fluid Mechanics **41**, pp. 181-202.
[23] Nishino, T., Roberts, G.T., and Zhang, X., 2008, "Unsteady RANS and detached-eddy simulations of flow around a circular cylinder in ground effect," Journal of Fluids and Structures **24**, pp. 18-33.
[24] Mockett, C., Perrin, R., Reimann, T., Braza, M., and Thiele, F., 2009, "Analysis of Detached-Eddy Simulation for the Flow around a Circular Cylinder with Reference to PIV Data," IUTAM Symposium on Unsteady Separated Flows and their Control, IUTAM Bookseries **14**, pp. 417-427.
[25] Menter, F. R., and Kuntz, M., "Development and application of a zonal DES turbulence model for CFX-5," CFX-validation report, CFX-VAL17/0503.
[26] Wieselberger, C., 1921, "New data on the law of hydro- and aerodynamic resistance," Physikalische Zeitschrift **22** (in German), pp. 321-328.
[27] Stansby, P. K., 1974, "The effects of endplates on the base pressure coefficient of a circular cylinder," Aeronautical Journal **78**, pp. 36-37.
[28] Gerich, D., and Eckelmann, H., 1982, "Influence of end plates and free ends on the shedding frequency of circular cylinders," Journal of Fluid Mechanics **122**, pp. 109-121.
[29] Revell, A., Craft, T., and Laurence, D., 2008, "Turbulence Modelling of Strongly Detached Unsteady Flows: The Circular Cylinder," Advances in Hybrid RANS-LES Modelling, NNFM 97, pp. 279-288.
[30] Wu, J., Sheridan, J., Hourigan, K., and Soria, J., 1996, "Shear Layer Vortices and Longitudinal Vortices in the Near Wake of a Circular Cylinder," Experimental and Thermal Fluid Science **12**, pp. 169-174.
[31] Hunt, J.C.R., Wray, A.A., and Moin, P., 1988, "Eddies, stream, and convergence zones in turbulent flows," Center for Turbulent Research Report No. CTR-S88-193.
[32] Dunn, W., 2004, "Vortex Shedding from Cylinders with Step-Changes in Diameter in Uniform and Shear Flows," Ph.D. thesis, Department of Mechanical Engineering, University of Ottawa, Canada.

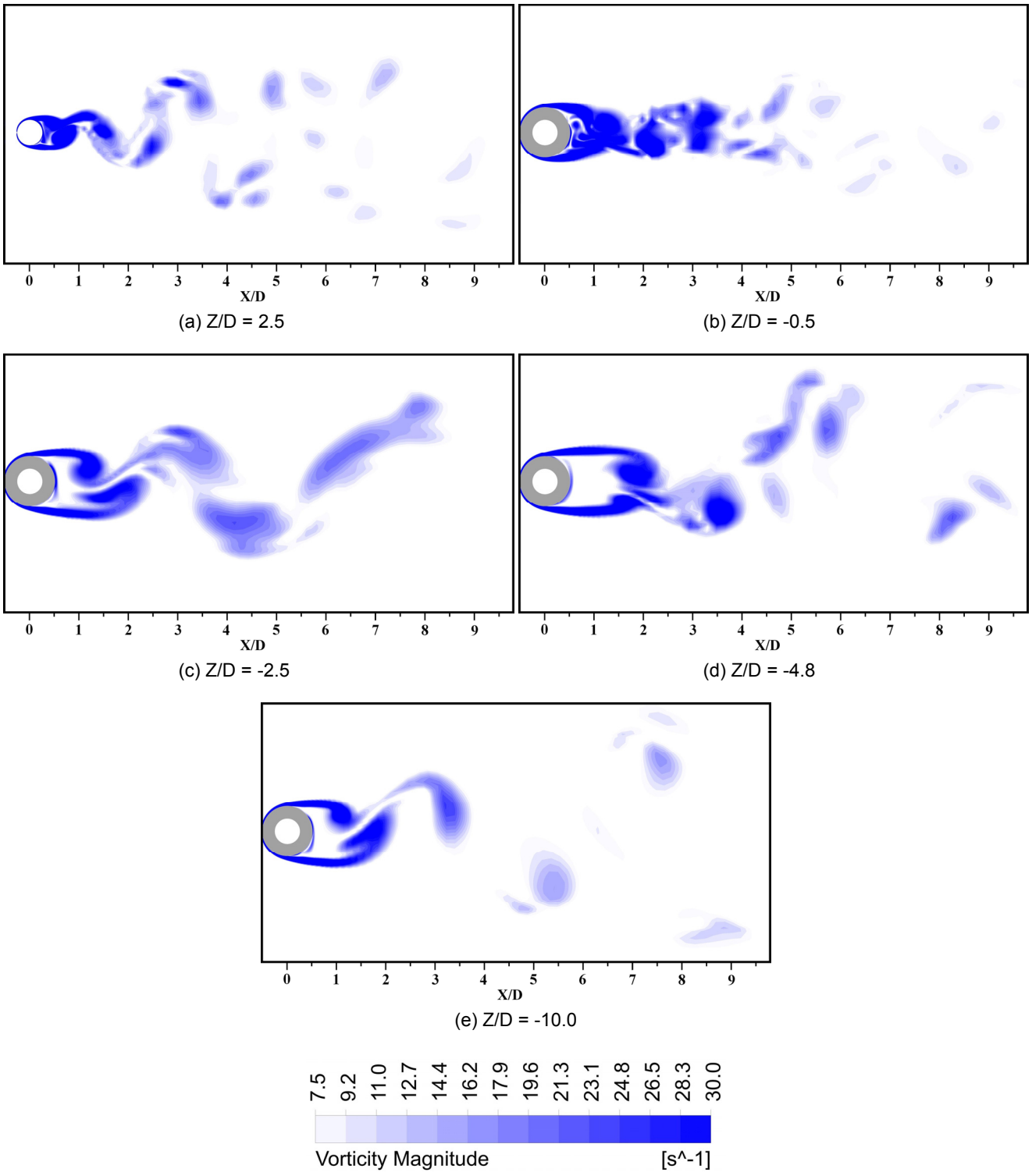

FIG 13. CHANGES IN THE VORTEX SHEDDING PATTERN ALONG THE SPAN OF THE STEP CYLINDER. THE PLOTS SHOW CONTOURS OF TOTAL VORTICITY MAGNITUDE.